Solar-Terrestrial Physics. 2024. Vol. 10. Iss. 2. P. 102–110. DOI: 10.12737/stp-102202410. © 2024 S.N. Ponomarchuk, V.P. Grozov. Published by INFRA-M Academic Publishing House

UDC 621.371.3, 621.376.3
DOI: 10.12737/stp-102202410

Received January 31, 2024
Accepted March 28, 2024

AUTOMATIC INTERPRETATION OF OBLIQUE SOUNDING IONOGRAMS BASED ON HYBRID ALGORITHMS

S.N. Ponomarchuk
Institute of Solar-Terrestrial Physics SB RAS, Irkutsk, Russia, spon@iszf.irk.ru

V.P. Grozov
Institute of Solar-Terrestrial Physics SB RAS, Irkutsk, Russia, grozov@iszf.irk.ru

Abstract. The paper presents a method of interpreting data on oblique ionosphere sounding (OS) with a continuous chirp signal. Hybrid algorithms for automatic interpretation of ionograms by selected points with significant amplitude obtained during secondary data processing for various heliogeophysical conditions have been developed and implemented. For the conditions of the two-layer ionosphere, an interpretation method has been worked out which involves analyzing histograms for the distribution of points with significant amplitude, which fall into a model mask constructed from the results of modeling of the distance-frequency characteristic for propagation when it moves over the ionogram. For the multilayer ionosphere, the interpretation is based on the study of the ionogram amplitude relief. The algorithms for extracting tracks of signals reflected from sporadic layers are examined separately. We present the results of interpretation of ionograms obtained on the network of chirp sounding radio paths in the northeastern region of Russia.

Keywords: ionosphere, ionogram, radio wave propagation, oblique ionosphere sounding.

INTRODUCTION

The effectiveness of HF radio systems depends on the matching between parameters of technical facilities and changing properties of the propagation medium, hence the need to equip radio centers with ionospheric diagnostic tools. One of these tools is a spatially-distributed chirp ionosonde operating in the oblique sounding (OS) mode [Ivanov et al., 2003; Podlesny et al., 2013]. Modern OS chirp ionosondes are widely used for studying and monitoring the ionosphere over long paths, including round-the-world ones, under various heliogeophysical conditions [Ivanov et al., 1997; Kurkin et al., 2000; Ivanov et al., 2003; Vertogradov et al., 2008]. The results of OS signal recording and processing in the chirp ionosonde's receiver are employed to form an ionogram [Podlesny et al., 2014]. When developing a system for diagnosing and predicting the ionosphere and HF radio wave propagation conditions on the basis of the OS ionosonde, it is important to automate experimental data processing and analysis in near real time. The key objective is to automatically interpret OS ionograms for near-real-time determination of the mode composition and maximum usable frequency (MUF) of each mode, to scale the predicted distance-frequency characteristics (DFC) of propagation modes, and to form tracks by significant points of the amplitude relief of a recorded signal. The MUF time series serve as initial data for near-real-time and short-term forecasting of radio wave propagation [Ilyin et al., 2018]. The selected signal tracks with a controlled signal-to-noise ratio are input data in algorithms for selecting the range of optimum working frequencies along communication radio paths [Vertogradov et al., 2008]. Reconstructing the vertical electron density distribution along tracks of 1F2 mode, identified in the OS ionogram, enables us to determine the main ionospheric parameters in a region remote from the transmitter and receiver [Mikhailov, Grozov, 2013; Ponomarchuk et al., 2015].

The purpose of this work is to develop and study methods for automatic interpretation of OS ionograms, obtained by the chirp ionosonde, in order to identify and form tracks of recorded signals under different heliogeophysical conditions. Algorithms for interpreting OS ionograms are based on the results of modeling of DFC of signal OS in the long-term prediction mode and on the results of secondary processing of experimental data on amplitude relief. The choice of an algorithm for interpreting ionograms depends on heliogeophysical conditions of radio wave propagation. For a two-layer ionosphere, an interpretation method is adopted which relies on the analysis of histograms of distribution of points with significant amplitude, which, due to signal delay, fall into a model mask constructed from the results of modeling of propagation mode DFC [Grozov et al., 2012]. For a multilayer ionosphere, signals are interpreted by examining the ionogram amplitude relief. Algorithms for isolating signal tracks reflected from the sporadic E_s layer are examined separately. We present the results of interpretation of ionograms obtained at the network of chirp sounding radio paths in north-eastern Russia.

EXPERIMENT AND DATA PROCESSING

To verify the ionogram processing and interpretation algorithms listed below, we have used the data acquired by the spatially distributed chirp ionosonde developed at ISTP SB RAS [Kurkin et al., 2024]. Transmitting stations are located near Magadan (60° N, 150.7° E), Khabarovsk (47.6° N, 134.7° E), in Norilsk (69.4° N, 88.4° E); the receiving station Irkutsk, in Tory village, Buryatia (51.8° N, 103° E). All the stations are equipped with

timing and synchronization devices. Transmitters and receivers are controlled automatically by preset operating mode programs. Transmitting and receiving chirp ionosondes form a network of ionospheric OS paths covering north-eastern Russia [Kurkin et al., 2024].

The ISTP SB RAS digital chirp ionosonde records signals according to the scheme for restoring the transfer function of radio channel [Podlesny et al., 2014]. The expression for the received signal $u_a(t)$ has the form

$$u_a(t) = H(\omega_0 + \eta t). \quad (1)$$

Here $H(\omega)$ is the transfer function of radio channel; ω_0 is the initial circular sounding frequency; η is the frequency deviation rate. To form an ionogram, digital signal samples that correspond to the expected delays in recorded signal arrival are multiplied by a smooth short time function (time window) and then the product spectrum is calculated. The received spectrum is a response of the radio channel to an effective narrowband complex signal whose shape, as function of time, is equal to the shape of the window spectrum, and the carrier frequency is related through the frequency deviation rate to the position of the window in the time sweep of the signal. Thus, at the output of the receiver, an OS ionogram is formed — a matrix, where each element (amplitude) $A(f_i, P_j)$ is determined by two characteristics: the group path (signal delay) P_j and the frequency f_i. The OS ionogram characterizes the frequency dependence of the group signal propagation time.

Figure 1 presents an OS ionogram obtained along the sounding path Khabarovsk—Irkutsk on July 7, 2015 at 04:51 UT. Unlike an analog ionosonde, a digital one processes data with a correction filter, which makes it possible to effectively detect spot interference and eliminate them without compromising the desired signal during primary processing [Podlesny et al., 2014].

To isolate an array of points corresponding to the moments of arrival of signals with significant amplitude relative to the signal-to-noise ratio, secondary processing of the ionogram is performed [Grozov et al., 2012; Penzin et al., 2019] which reduces to solving two problems:

- preprocessing of ionograms to eliminate noise from an image and improve amplitude characteristics;
- data compression allowing a significant reduction in their volume without appreciable loss of useful information.

To remove noise from an image and recover signal samples at intermediate points, we employ a median filter capable of smoothing noise and reducing blurring of track boundaries, as well as restoring values in track breaks.

The mechanism of cellular automaton is used to eliminate single artifacts, partially recover data, and identify the primary track in the ionogram [Grozov et al., 2012; Penzin et al., 2019]. After secondary processing of the OS ionogram, a new matrix of experimental points $A(f_i, P_j)$ is formed which corresponds to an array of points with significant amplitude $(f, P, A)_k$ $k = \overline{1, M}$.

Figure 2 illustrates the results of secondary processing of the OS ionogram shown in Figure 1, as well as the results of calculation of signal propagation DFC

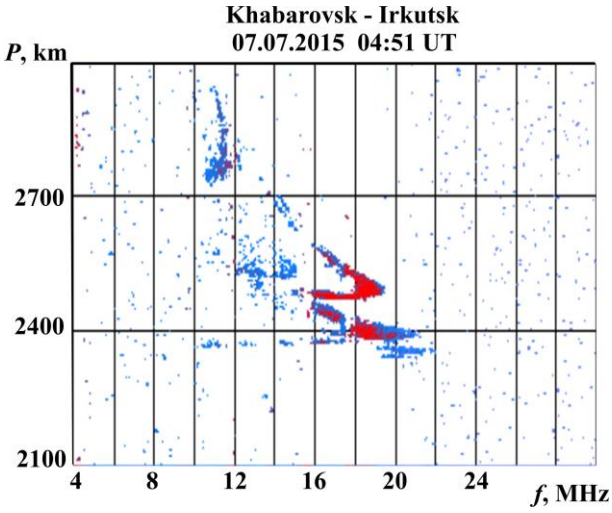

Figure 1. OS ionogram: July 07, 2015, 04:51 UT

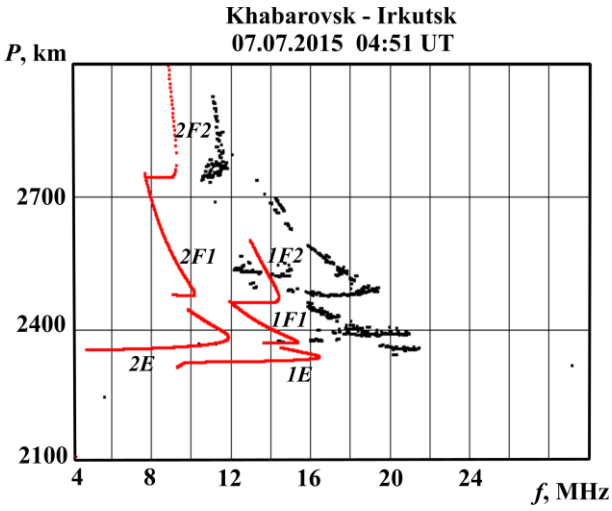

Figure 2. Results of OS ionogram processing and *P(f)* modeling on July 07, 2015, 04:51 UT. Black dots represent the processing results; red dots, *P(f)*

$P_l^j(f)$. Here P is the group path; l is the number of reflections from the ionosphere; j is the propagation channel number (its lower wall is the Earth surface, and the upper one is an ionospheric layer); for waveguide channels E, F1, F2 j=1, 2, 3 respectively. Calculations of $P_l^j(f)$ have been carried out by the transmission curve method [Davies, 1973; Kotovich et al., 2006], using the height-frequency characteristic (HFC) of vertical sounding, calculated at a midpoint of a radio path by the operational semi-empirical model of the ionosphere. The operational HFC model was developed at ISTP SB RAS by decomposing the HFC nodal parameters: f_oE, f_oF1, f_o F2, h'F, h'F2, h_pF, h'F1 by natural orthogonal functions (NOFs) [Dvinskikh, 1988].

The modeling $P_l^j(f)$ allows us to identify individual recorded signals in an ionogram. In the OS ionogram shown in Figure 2, we can quite confidently identify signals related to propagation modes 1F1, 1F2, and 2F2. The identification of 1E mode is ambiguous because of the presence of signals reflected from the sporadic E_s layer in the ionogram.

INTERPRETATION OF IONOGRAMS

The main purpose of interpreting OS ionograms in near real time is to identify the mode composition, determine MUF of each mode, $f_{m,l}^{j}$, correct frequency dependences of the group propagation path $P_l^j(f)$, and form signal tracks at points with significant amplitude. The ionogram interpretation results can be utilized as input parameters

- when choosing the range of optimum working frequencies for a given radio path from current OS data [Vertogradov et al., 2008];
- when solving the inverse problem of determining ionospheric parameters from OS data [Kotovich et al., 2006; Krasheninnikov et al., 1990; Mikhailov, Grozov, 2013; Ponomarchuk et al., 2015; Song et al., 2016].

Conventionally, OS ionograms can be divided into three types: ionograms obtained 1) in winter, spring, and fall and at night in summer; 2) during daytime in summer; 3) during strong ionospheric disturbances.

Ionograms of the first type in the absence of ionospheric disturbances feature a fairly simple mode structure of received signals. The main traces of reflections in OS ionograms correspond to the signals arriving at a receiving point through reflection from the ionospheric F2 layer. An ionogram of the first type is shown in Figure 3. It was obtained along the Magadan—Irkutsk path on January 15, 2023 at 09:00 UT. Dashed black lines are the results of modeling of OS DFC *P*(*f*), which allow us to identify in the ionogram the signals that arrive at the receiver through single, double, and triple reflections from the F2 layer, — 1F2, 2F2, and 3F2 respectively. The mode received-signal structure becomes more complex in the presence of large-scale ionospheric irregularities along the radio wave propagation path. Figure 4 exemplifies an OS ionogram along the Khabarovsk—Irkutsk path, obtained on January 4, 2014 at 02:16 UT. Signals 1F2, 2F2, and 3F2 are identified in the ionogram. The signals reflected from the E layer are faint — the frequency range is 8–12 MHz. There are so-called m-modes between main propagation modes 1F2 and 2F2, 2F2 and 3F2 due to various combinations of the main reflection from the F2 layer with intermediate reflections from the E layer (represented by m) [Davies, 1973, Blagoveshchensky et al., 2018]. If traveling ionospheric disturbances (TIDs) occur along the radio path, there are sickle-shaped tracks corresponding to reflections from medium-scale TIDs in the upper Pedersen ray of main propagation mode 1F2 [Kurkin et al., 2024] (TID arrow).

An example of the second-type ionogram is the OS ionogram obtained along the Khabarovsk—Irkutsk path on July 7, 2015 at 04:51 UT (see Figure 2). The multilayer structure of the ionosphere gives rise to additional signals, reflected from the F1 layer, in OS ionograms. A distinctive feature of the summer daytime OS ionograms is the presence of pronounced traces corresponding to delays in the arrival of signals reflected from the sporadic E_s layer. During some summer daytime periods, the E_s layer becomes dominant along the path, which leads

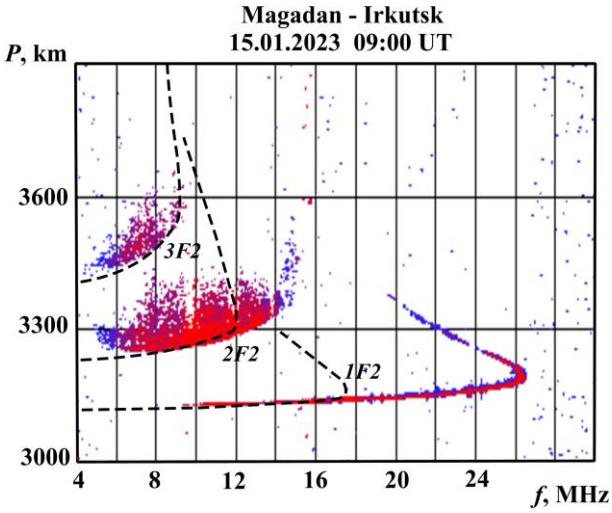

Figure 3. OS ionogram and model results for *P*(*f*): January 15, 2023, 09:00 UT. The black dashed line is *P*(*f*)

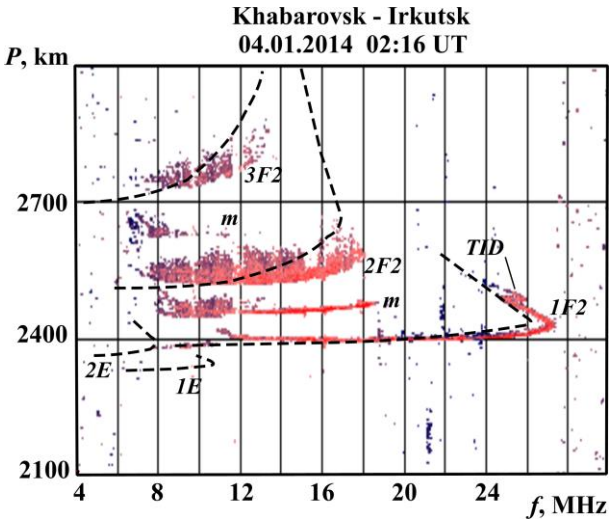

Figure 4. OS ionogram and model results for *P*(*f*) on January 04, 2014, 02:16 UT. The black dashed line is *P*(*f*)

to complete shielding of the overlying reflecting ionospheric layers F1 and F2. The maximum operating frequency for receiving signals reflected from the E_s layer may exceed the maximum frequency of the transmitter. During the summer period, medium-scale TIDs and m-propagation modes are also regularly recorded.

The third type includes ionograms obtained during ionospheric disturbances, caused mainly by strong magnetic storms. During geomagnetic disturbances, the auroral oval and the main ionospheric trough (MIT) shift to lower latitudes, thereby affecting the mode structure of the signal [Uryadov et al., 2004; Blagoveshchensky et al., 2018]. Ionospheric irregularities of different scales near the southern auroral oval boundary give rise to significant variations in the maximum observed frequency (MOF) [Kurkin et al., 2008], to an increase in the diffusivity of signals of standard propagation modes, and to the occurrence of additional signals with delays exceeding the delays of the main modes propagating along the great-circle arc. Interpreting these signals requires special methods of calculating propagation characteristics and ionospheric models including large-scale

structures such as MIT and irregularity models. The problem of interpreting ionograms of the third type is therefore out of the scope of this paper.

The OS ionogram interpretation method is based on using the results of modeling $P_l^j(f)$ along a given path in the long-term prediction mode and processing of experimental ionograms $(f, P, A)_k$ $k = \overline{1, M}$ [Grozov et al., 1996; Ponomarchuk et al., 2013]. The method relies on adiabatic invariants — values retained during variations in ionospheric parameters within the long-term prediction error (20 %), namely,

- the ratio of the group path $P_{m,l}^j$ at the junction of the lower and upper rays to the distance length $D\,\gamma = P_{m,l}^j / D$;
- the frequency dependence of the group path of the $P_l^j(f)$ mode on the relative frequency grid $\beta = f / f_{m,l}^j$, where $f_{m,l}^j$ is the MUF mode for the distance considered $P_l^j(\beta)$;
- the ratio of MUF modes of different multiplicities propagating in one of the waveguide channels $\chi = f_{m,l}^j / f_{m,l\pm1}^j$.

Let us examine the OS ionogram interpretation algorithm of the first type. First, the separation of signal modes is carried out. To do this, $P_l^j(f)$ is calculated for a given path in the long-term prediction mode. The calculation results are used to create a model mask for the mode of minimum multiplicity $l_{\min}$ of the F layer, including two bands of vertical width ΔP (km): 1) for the lower ray with a frequency from μf_m^p to f_m^p, where f_m^p is the predicted MUF of the reference mode; 2) for the upper ray with a frequency from νf_m^p to f_m^p. The μ and ν values can be varied (empirically selected values $\mu \cong 0.7$, $\nu \cong 0.8$). Figure 5 depicts a mask of one-hop mode 1F2 on the relative frequency grid $\beta = f / f_{m,1}^3$ for the OS ionogram obtained on January 15, 2023 at 09:00 UT (see Figure 3). The blue line indicates the results of $P_1^3(f)$ calculation of 1F2; black dots mark the results of secondary ionogram processing; and the red dashed line shows the position of the long-term prediction model mask.

The algorithm for identifying the reference mode (minimum multiplicity mode) in the ionogram consists in counting the number of points with significant amplitude in the model mask on the relative frequency grid as it moves over the ionogram. The mask moves without turns by combining the nose of the mask with significant-amplitude points $(f, P, A)_k$, $k = \overline{1, M}$. When in motion, the number of points N_k falling into the mask within rectangles $\Delta f \times \Delta P$ centered at each point of the mask is calculated, where Δf and ΔP are selected based on the range and frequency resolutions of the ionosonde. The values of frequency f_m^r and group path P_m^r at which the number of points falling into the mask is maximum are taken as real MUFs and as the closing point of the upper

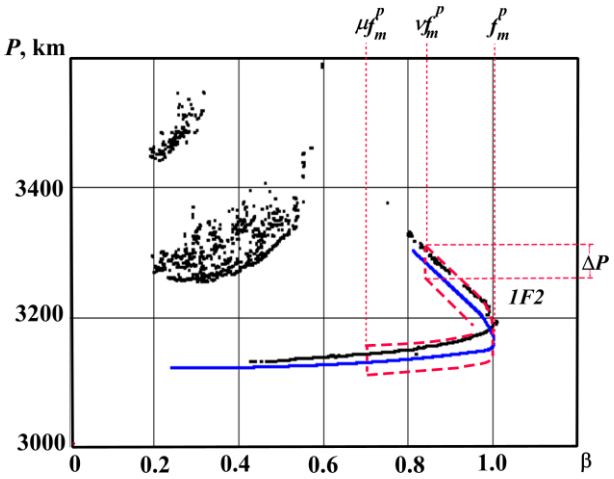

Figure 5. Results of OS ionogram processing and mode model mask 1F2 on the relative frequency grid β for January 15, 2023, 09:00 UT. Black dots represent the processing results; the red dashed line is the mask

and lower rays of the propagation mode. If the maximum number of points falling into the mask is smaller than a certain number, it is assumed that the multiplicity mode $l_{\min}$ has not been identified and the procedure is repeated for $l_{\min}$+1. The transition to $l_{\min}$+1 must also be made if the reference mode goes beyond the right edge of the ionogram — the mode MUF is higher than the maximum sounding frequency. Therefore, before identifying the reference mode, it is required to scan the right edge of the ionogram by a rectangular mask with horizontal and vertical dimensions of ~1000 kHz and ΔP respectively. In this case, the propagation mode can also be interpreted using the recorded tracks for the lower and upper rays falling into the model mask.

When f_m^r and P_m^r are determined, $P^{\text{mod}}(f)$ is corrected through frequency scaling by a multiplier f_m^r / f_m^p; hence, we obtain the frequency dependence of the group path $P^{\text{real}}(f)$, which is used to form a track for the interpreted propagation mode. To do this, from $(f, P)_k$, $k = \overline{1, M}$ points are selected that fall into bands ΔP wide along the frequency dependence line of the group path $P^{\text{real}}(f)$, tied to the point $\left(f_m^r, P_m^r\right)$. Then, the track points are linearly interpolated on a uniform frequency grid.

Higher-multiplicity modes and propagation modes in other channels are interpreted by an identical algorithm. To increase the performance of the algorithm for constructing a histogram of the number of points falling into the model mask, approximate values f_m^r and P_m^r are found using adiabatic invariants $\gamma = P_{m,l}^j / D$ and $\chi = f_{m,l}^j / f_{m,l\pm1}^j$. Thus, local regions within which the model mask moves are isolated in the ionogram.

The developed scheme for interpreting propagation modes makes it possible to restore $P^{\text{real}}(f)$ of OS signals along a given path when there are no standard propagation modes or problems arise in their identification due to multipath propagation and diffusivity. $P^{\text{real}}(f)$ is restored as follows. We calculate $P_l(f)$ by the predictive ionospheric model and the predictive adiabatic ratio of

mode MUFs of different multiplicities, $\chi = f^{p}_{m,l} / f^{p}_{m,l\pm1}$, where l is the multiplicity of the mode present in the ionogram. Next, the experimental MUF of the l mode $f^{r}_{m,l}$ is determined and the values $f^{r}_{m,l\pm1} = f^{r}_{m,l} / \chi$ are calculated. After determining real MUFs and having calculations of the group path from predicted ionospheric parameters, we can restore OS $P^{\text{real}}_{l\pm1}(f)$ of absent modes on the relative frequency grid $\beta = f / f^{p}_{m,l\pm1}$ for the current time by multiplying β by $f^{r}_{m,l\pm1}$.

Signals corresponding to reflections from the E layer in ionograms of the first type, except for the summer period of the year, are recorded in a narrow frequency range, and their amplitudes are low. The points with significant amplitude selected by processing and corresponding to the lower rays for the E and F propagation modes are close in delay in the low-frequency region, so their separation in automatic mode is difficult. In summer, tracks of signals reflected from the E layer can be isolated and identified using the model mask based on a long-term forecast $P^{1}_{l}(f)$. At the same time, the E-mode track transforms to the E_s-mode track; therefore, their separation is also difficult.

To interpret signals reflected from the E_s layer, a procedure is adopted for identifying points with significant amplitude for signals with an almost constant delay in the selected group path corridors in OS ionograms. For radio paths shorter than 3000 km, boundaries of the corridors can be calculated within the flat Earth—ionosphere waveguide, using the equivalence theorem in the modified transmission curve method. The angle of incidence φ of a ray on a layer according to the equivalence theorem in the modified transmission curve method is related to the current height h' by the following formula [Kotovich et al., 2006]:

$$\varphi = \operatorname{arctg}\left(\frac{\sin\left(D/(2R)\right)}{x - \cos\left(D/(2R)\right)} \right), \qquad (2)$$

where $x = \dfrac{R + h'}{R}$; R is the Earth radius. The signal group path P at oblique propagation is determined as follows:

$$P = 2R \frac{\sin(\Omega - \varphi)}{\sin\varphi}, \qquad (3)$$

where $\Omega = \arcsin(x \sin\varphi)$. Suppose that the equivalent height at which the E_s layer is located at the midpoint of the path is 105 km. From Formula (3) calculate the group path P_n with a signal reflection at 105 km for the first and second jumps if the path length is shorter than 2000 km, and for the second and third jumps if the path is longer than or equal to 2000 km. With these boundaries, signal tracks are formed from an array of points with significant amplitude $(f, P, A)_k$, $k = \overline{1, M}$ in the selected group path corridors. The tracks are interpreted taking into account the number of reflections from the E_s layer. From the selected E_s tracks MOF and the group path for each track are determined. If there are areas of track absence with a frequency width over 400 kHz, the left and right boundaries of the frequency range are selected within the continuity of the track. If such areas are less than 400 kHz, the initial and final boundaries of E_s are chosen from the extreme values of the track frequency.

Figure 6 presents the results of processing of the OS ionogram obtained along the Magadan — Irkutsk path on January 15, 2023 at 09:00 UT, and the results of automatic interpretation of propagation modes 1F2, 2F2, and 3F2. Gray dots are the results of the OS ionogram processing; red dots are the results of recovery of frequency dependences of the group path $P^{\text{real}}(f)$; blue dots are the selected signal tracks. Figure 7 shows the results of processing and interpretation of the OS ionogram obtained along the Magadan—Irkutsk path on August 11, 2014 at 00:00 UT. The interpretation results of propagation modes 2E, 1F2, and 2F2 are marked with red dots; the results of ionogram processing, with gray dots; and the results of track selection, with blue dots. Unlike winter conditions,

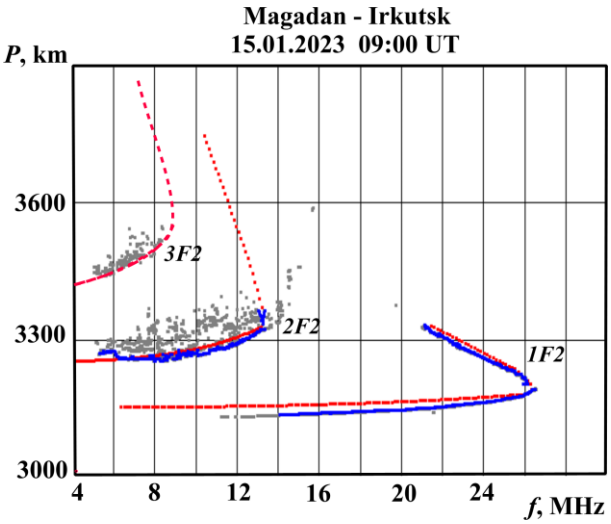

Figure 6. Results of processing and interpretation of the OS ionogram obtained on January 15, 2023 at 09:00 UT. Gray dots represent processing results; red dots, $P^{\text{real}}(f)$; blue dots, signal tracks

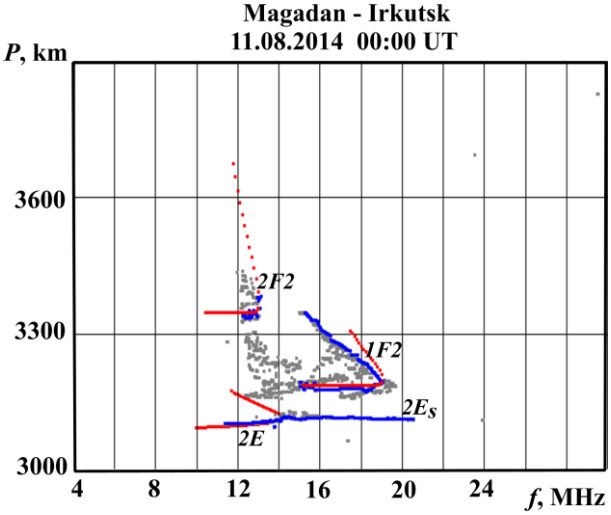

Figure 7. OS ionogram obtained on August 11, 2014 at 00:00 UT. Designations are the same as in Figure 6

in summer the signals reflected from the E_s layer are recorded in the OS ionogram in the morning. The selected and automatically identified track of $2E_s$ mode is marked with blue dots.

The main difficulties in automatic interpretation of OS ionograms arise in summer under conditions of radio wave propagation in the multichannel Earth—ionosphere waveguide formed by the multilayer ionosphere and the Earth surface. The mode structure of received signals becomes more complex even in the absence of ionospheric disturbances of different types. Along with standard modes of propagation from the ionospheric E and F layers there are m-modes and signals reflected from the E_s layer in OS ionograms. The above ionogram interpretation scheme based on construction of model masks from a long-term forecast is difficult to adopt owing to two main reasons. It is necessary to have a) ionospheric models that adequately describe the vertical electron density distribution in the vicinity of the F1 layer and in the lower ionosphere; b) operational algorithms for calculating the trajectory characteristics of propagation in a multilayer anisotropic ionosphere. Additional difficulties arise in classifying signals, reflected from the E_s and F1 layers, by group delay.

A hybrid algorithm that involves analyzing amplitude characteristics of a received signal has been developed to interpret summer OS ionograms. The amplitude-frequency dependence $\Phi(f)=\sum_j A^2(f_i, P_j)$ (summation over points P_j at a fixed frequency f_i) and the amplitude-distance characteristic $\Psi(P)=\sum_i A^2(f_i, P_j)$ (summation is made by points of frequency range f_i for a fixed group path P_j) are calculated. Let us examine the main elements of the interpretation algorithm, using the OS ionogram obtained along the Khabarovsk—Irkutsk path on July 7, 2015 at 04:51 UT and shown in Figure 1, as an example. Figure 8 presents the results of secondary processing of the OS ionogram, the dependences $\Phi(f)$ and $\Psi(P)$, and the calculated corridor boundaries for signals reflected from

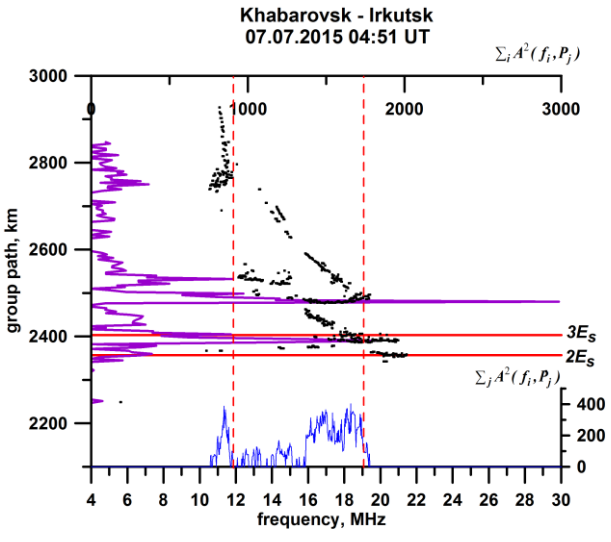

Figure 8. Gray dots indicate an OS ionogram; the blue line, $\Phi(f)$; the dark-red line, $\Psi(P)$; red lines are E_s boundaries

the E_s layer. Points with significant amplitude are marked in gray; red lines are the lower boundaries of the arrival corridors of two-hop and three-hop modes of propagation by reflecting from the E_s layer; the dependences $\Psi(P)$ and $\Phi(f)$ averaged over three points are indicated by dark-red and blue lines respectively. The amplitude-distance characteristic $\Psi(P)$ is calculated by $(f,\ P,\ A)_k, k=\overline{1, M}$. The method of calculating $\Phi(f)$ is described below.

Local maxima in $\Psi(P)$ show the location of signals, reflected from different ionospheric layers, in the ionogram. According to the results of $P_l^j(f)$ calculation from the long-term forecast and the calculation of the arrival corridors of signals reflected from the E_s layer, we can pre-identify signal tracks in the ionogram from $\Psi(P)$. The first maximum in $\Psi(P)$ corresponds to the arrival time of a one-hop signal reflected from the E or E_s layers — mode 1E or $1E_s$; the second maximum, to two-hop mode $2E_s$ and one-hop mode 1F1; the third maximum, to mode 1F2. With the boundaries of the E_s channels and the results of the long-term forecast of $P_l^1(f)$, tracks of signals reflected from the E and E_s layers are formed from the array of high-amplitude points $(f,P,A)_k\, k=\overline{1, M}$. If there are E modes in the long-term forecast of $P_l^1(f)$, the model mask method determines MUF of the minimum multiplicity mode $l_{\min}$, corrects model DFC $P_{l\min}^1(f)$, and forms the E-mode track. From the remaining points with significant amplitude, tracks of signals reflected from E_s are formed and identified. The identified tracks define the right E_s-layer frequency boundary $f_{m,Es}$ and the maximum group path P_{Es} of signals reflected from E and E_s.

Then, the regions are found in the ionogram in which signals reflected from the F1 and F2 layers by the model mask method are identified and interpreted. To do this, the ionogram is cut from below by P_{Es}, i.e. a new array of points with significant amplitude is formed $(f, \tilde{P}, A)_n, n=\overline{1, N}$ in which $\tilde{P} > P_{Es}, N<M$. The new array of points with significant amplitude is used to compute $\Phi(f)=\sum_j A^2(f_i, \tilde{P}_j)$. Analysis of $\Phi(f)$ allows us to identify MOFs of the frequency propagation modes relative to the given initial level of signal amplitude depending on the signal-to-noise ratio. In Figure 8, vertical dashed lines indicate MOFs for 1F1, 1F2, and 2F2 modes equal to 19.3 and 11.9 MHz respectively. The intersection point of the vertical line of MOF with the horizontal line corresponding to the local maximum of $\Psi(P)$ allows us to determine the approximate location of the closing point of the upper and lower rays and MUF for propagation modes 1F1, 1F2 or 2F2. Further, the model mask algorithm is employed to more accurately identify MUFs of modes, correct predicted $P_1^2(f)$, $P_1^3(f)$, $P_2^3(f)$, and form signal tracks.

Figure 9 exhibits an OS ionogram, obtained along the Khabarovsk—Irkutsk path, on July 7, 2015 at 04:51 UT, with the results of interpretation and formation of tracks of propagation modes $1E_s$, $2E_s$, 1F1, 1F2, and 2F2.

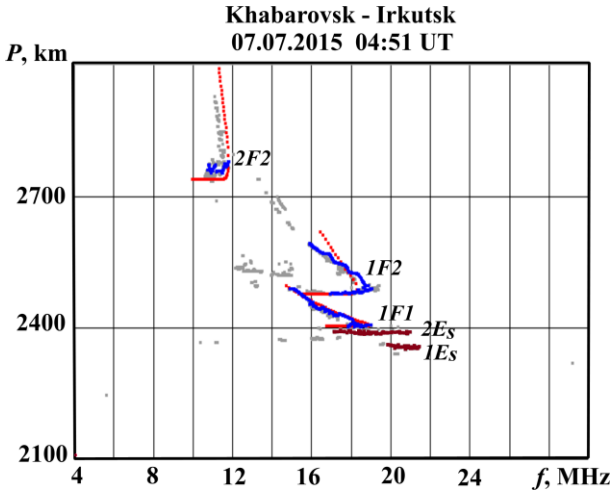

Figure 9. Results of processing and interpretation of the OS ionogram obtained on July 07, 2015 at 04:51 UT. Gray dots indicate processing results; red dots, $P^{real}(f)$; blue dots, signal tracks

Gray dots are the moments of arrival of signals with significant amplitude; red dots are the results of interpretation of propagation modes $P^{real}(f)$; dark-red dots are $1E_s$ and $2E_s$ tracks; blue dots, 1F1, 1F2, and 2F2 tracks.

INTERPRETATION RESULTS

The developed algorithms for automatic processing and interpretation of OS ionograms have been tested on a large array of experimental data acquired in northeastern Russia in the Magadan — Irkutsk, Khabarovsk — Irkutsk, Norilsk — Irkutsk radio path network [Kurkin et al., 2008]. To assess the reliability, relative errors $\delta = \left(f_m^{\text{manual}} - f_m^{\text{a}} \right) / f_m^{\text{manual}} \cdot 100\,\%$, were calculated where f_m^{manual}, f_m^{a} are propagation mode MOFs obtained due to manual and automatic processing of ionograms respectively. Figures 10, 11 illustrate distributions of the relative error in determining MOF of 1F2 mode along the Khabarovsk—Irkutsk and Magadan—Irkutsk paths in March 2014. The general sample for each month contains 8928 ionograms.

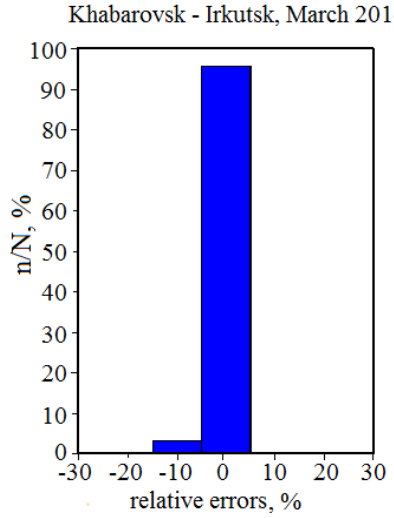

Figure 10. Distribution of relative errors in determining MOF of 1F2 mode along the Khabarovsk—Irkutsk path in March 2014

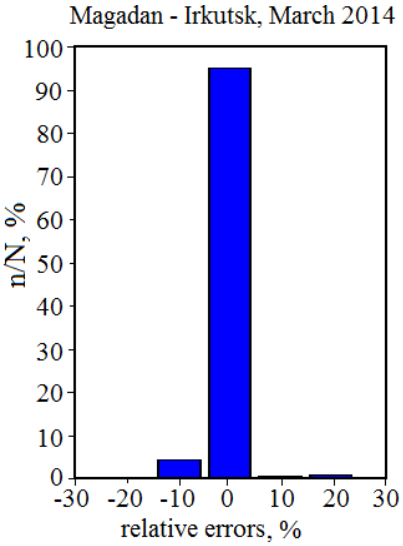

Figure 11. The same as in Figure 10 for the Magadan—Irkutsk path in March 2014.

Figure 12 shows diurnal variations in the limit frequency MOF_{Es} of signal reflection from the E_s layer along the Magadan—Irkutsk path on July 11, 2015. Black and red dots are the results of manual and automatic processing of OS ionograms. Figures 13, 14 depict diurnal variations in MOFs of propagation modes 1F1 and 1F2 respectively (MOF_{1F1} and MOF_{1F2}) along the Magadan—Irkutsk path on July 11, 2015. Figures 15–17 exhibit diurnal variations

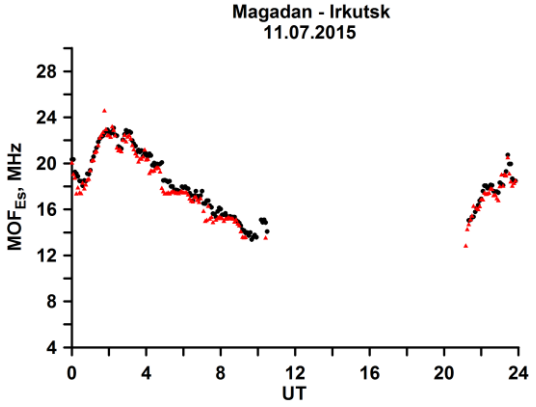

Figure 12. Diurnal variations in the limit frequency of the MOF_{Es} mode along the Magadan—Irkutsk path on July 11, 2015. Black and red curves indicate manual and automatic processing

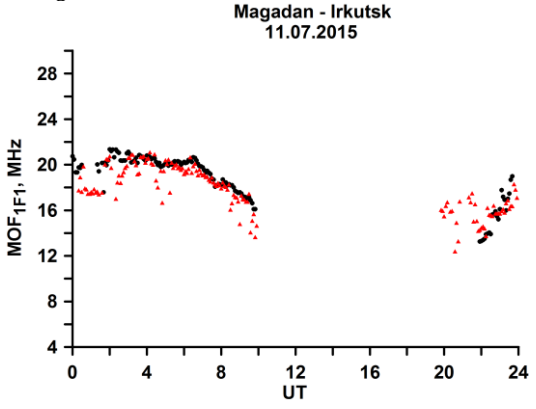

Figure 13. The same for MOF_{1F1}

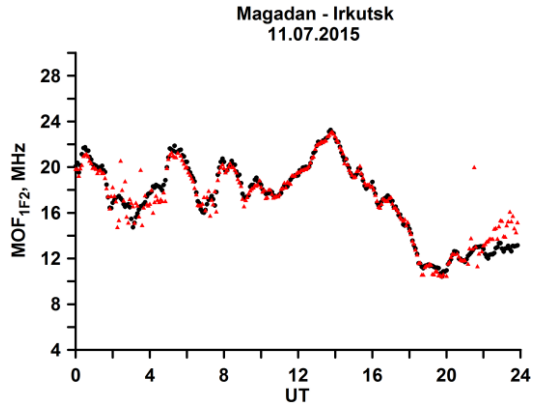

Figure 14. The same for MOF_{1F2}

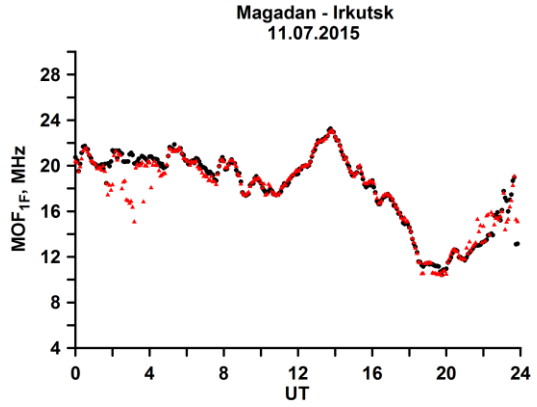

Figure 15. The same for MOF_{1F}

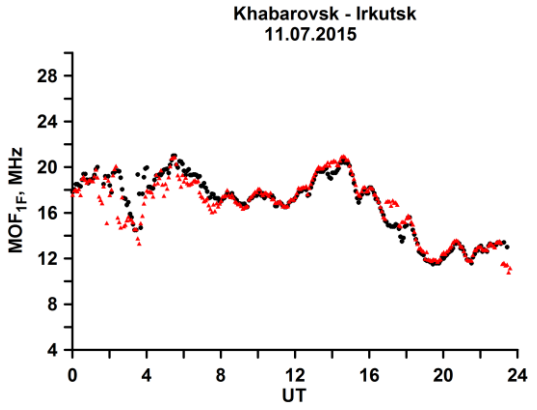

Figure 16. The same for MOF_{1F} along the Khabarovsk—Irkutsk path

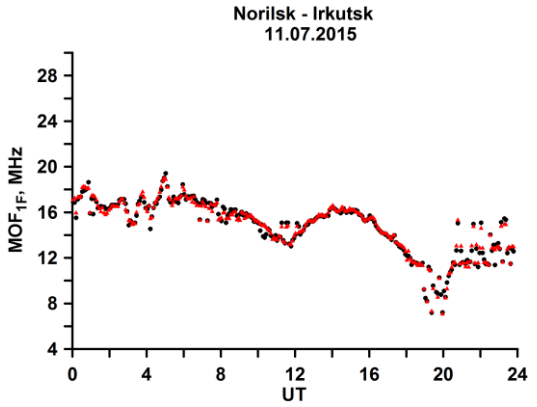

Figure 17. The same for MOF_{1F} along the Norilsk—Irkutsk path

Standard deviations of relative errors in determining propagation modes, %

Date	Magadan—Irkutsk				Khabarovsk—Irkutsk			
	MOF_{Es}	MOF_{1F1}	MOF_{1F2}	MOF_{1F}	MOF_{Es}	MOF_{1F1}	MOF_{1F2}	MOF_{1F}
August 2014	6.89	7.34	5.78	6.21	6.11	3.25	3.67	5.83
July 2015	5.54	6.15	7.27	4.0	9.56	10.26	8.45	6.87

in MOF_{1F}=max(MOF_{1F1}, MUF_{1F2}) during this period along the Magadan—Irkutsk, Khabarovsk—Irkutsk, and Norilsk—Irkutsk paths respectively.

Table lists the results of testing the developed algorithms at the network of chirp sounding radio paths in summer — standard deviations of relative errors in determining MOFs of propagation modes in percent. The general sample for each month contains 8928 ionograms.

CONCLUSION

Thus, the developed methods of analyzing and interpreting OS ionograms allow for near-real-time automatic determination of the mode composition and MUFs of each mode, correction of propagation mode DFC, and formation of tracks of recorded signals at significant points in the ionogram amplitude relief. Output characteristics of the developed interpretation algorithms are: MOFs of 1F2, 2F2, 1F1 propagation modes; E_s-layer critical frequencies; identified signal tracks. New algorithms are those that separate signals reflected from the E_s, 1F1, and 1F2 layers by studying the amplitude-distance characteristic $\Psi(P)$ plotted by significant points of the amplitude relief. Algorithms for determining MOFs of the main propagation modes by analyzing the amplitude-frequency dependence $\Phi(f)$ for a given signal-to-noise ratio are also new.

The results of ionogram interpretation can be used in selecting optimum operating frequency ranges for a given radio path from current OS data; in solving the inverse problem of determining ionospheric parameters from OS data. Solving these problems requires improving the procedure for forming tracks of recorded signals from corrected OS DFC $P^{real}(f)$ in view of multipath propagation and scattering of signals by ionospheric irregularities and roughnesses of the Earth surface. In other words, it is necessary to achieve an optimal fit of the $P^{real}(f)$ curve to the cloud of experimental points with significant amplitude identified during secondary ionogram processing. The identified tracks of experimental points with a given signal-to-noise ratio can be utilized as input data in algorithms for selecting optimum operating frequencies (e.g., [Vertogradov et al., 2008]). To solve the inverse problem of determining ionospheric parameters from OS data, it is necessary to correctly identify the upper ray of single mode 1F2 in

order to more accurately define the F2-layer critical frequency.

The work was financially supported by the Ministry of Science and Higher Education of the Russian Federation (Subsidy No. 075-GZ/Ts3569/278). The experimental data was obtained using the equipment of Shared Equipment Center «Angara» [http://ckp-rf.ru/ckp/3056/].

REFERENCES

Blagoveshchensky D.V., Zhbankov G.A., Maltseva O.A. Observed and calculated ionograms of oblique ionospheric sounding on HF radio paths during a magnetic storm of September 7–8, 2017. *Radiophysics and Quantum Electronics.* 2019, vol. 61, no. 12, pp. 881–892.

Davies K. *Ionospheric Radio Waves.* Blaisdell, London, 1969, 460 p.

Dvinskikh, N.I. Expansion of ionospheric characteristics fields in empirical orthogonal functions. *Adv. Space Res.* 1988, vol. 8, no. 4, pp.179–187. DOI: 10.1016/0273-1177(88)90238-4.

Grozov V.P., V.I. Kurkin, V.E. Nosov, Ponomarchuk S.N. An interpretation of data oblique-incidence sounding using the chirp-signal. *Proceedings of ISAP`96, Chiba, Japan*. 1996, pp. 693–696.

Grozov V.P., Ilyin N.V., Kotovich G.V., Ponomarchuk S.N. Software system for automatic interpretation of ionosphere sounding data. *Pattern Recognition and Image Analysis*. 2012, vol. 22, no. 3, pp. 458–463.

Ilyin N.V., Bubnova T.V., Grozov V.P., Penzin M.S., Ponomarchuk S.N. Real-time forecast of MUF for radio paths from current data obtained from oblique sounding with continuous chirp signal. *Solar-Terr. Phys*. 2018, vol. 4, iss. 3, pp. 83–91. DOI: 10.12737/szf-43201811.

Ivanov V.A., Ryabova N.A., Shumaev V.V., Uryadov V.P. Forecasting and updating HF channel parameters on the basis of oblique chirp sounding. *Radio Sci.* 1997, vol. 32, no. 3, pp. 983–988.

Ivanov V.A., Kurkin V.I., Nosov V.E., Uryadov V.P., Shumaev V.V. Chirp ionosonde and its application in the ionospheric research. *Radiophysics and Quantum Electronics*. 2003, vol. 46, iss. 11, pp. 821–851.

Kotovich G.V., Kim A.G., Mikhailov S.Ya., Grozov V.P., Mikhailov Ya.S. Determining the f_0F2 critical frequency at the path midpoint from oblique sounding data based on the Smith method. *Geomagnetism and Aeronomy*. 2006, vol. 46, no. 4, pp. 517–521.

Krasheninnikov I.V., Liannoy B.E. Estimation of the true ionospheric height profile, with a continuous gradient, from oblique sounding data. *J. Atmos. Terr. Phys.* 1990, vol. 52, no. 2. pp. 113–117.

Kurkin V.I., Nosov V.E., Matyushonok S.M., Litovkin G.I., Ivanov V.L., Shumaev V.V., et al. The features of round-the-world signal propagation over the paths of the Russian chirp-sounder network during low and mild solar activity. *Radiophysics and Quantum Electronics*. 2000, vol. 43, iss. 10, pp. 755–765.

Kurkin V.I., Pirog O.M., Polekh N.V., Mikhalev A.V., Poddelsky I.N., Stepanov A.E. Ionospheric response to geomagnetic disturbances in the north-eastern region of Asia during the minimum of 23rd cycle of solar activity. *J. Atmos. Solar-Terr. Phys.* 2008, vol. 70, no. 18, pp. 2346–2357. DOI: 10.1016/j.jastp.2008.09.022.

Kurkin V.I., Medvedeva I.V., Podlesnyi A.V. Effect of sudden stratosphere warming on characteristics of medium-scale traveling ionospheric disturbances in the Asian region of Russia. *Adv. Space Res.* 2024, vol. 73, no. 7, pp. 3613–3623. DOI: 10.1016/j.asr.2023.09.020.

Mikhailov S.Y., Grozov V.P. Recovery of the Nonmonotonic Altitude Profile of the Plasma Frequency Based on the Ionospheric Oblique Sounding Data. *Radiophysics and Quantum Electronics*. 2013, vol. 56, iss. 7, pp. 399–412.

Penzin M.S., Ponomarchuk S.N., Grozov V.P., Kurkin V.I. Real-time techniques for interpretation of ionospheric backscatter sounding data. *Radio Sci*. 2019, vol. 54, iss. 5, pp. 480–491. DOI: 10.1029/2018RS006656.

Podlesnyi A.V., Brynko I.G., Kurkin V.I., Berezovskii V.A., Kiselev A.M., Petukhov E.V. Multifunctional chirp ionosonde for monitoring the ionosphere. *Geliogeofizicheskie issledovaniya* [Heliogeophys. Res.]. 2013, no. 4, pp. 24–31. (In Russian).

Podlesnyi A.V., Lebedev V.P., Ilyin N.V., Khahinov V.V. Implementation of the method for restoring the transfer function of the ionospheric radio channel based on the results of sounding the ionosphere with a continuous chirp signal. *Electromagnetic waves and electronic systems*. 2014, vol. 19, no. 1, pp. 63–70. (In Russian).

Ponomarchuk S.N., Grozov V.P., Kotovich G.V., Mikhailov S.Ya. The processing and interpretation of vertical and oblique sounding ionograms for ionosphere diagnostics on the base of chirp - ionosonde. *Bull. Siberian State Aerospace University named after. acad. M.F. Reshetneva,* 2013, no. 5 (51), pp. 163–166.

Ponomarchuk S.N., Grozov V.P., Kim A.G., Kotovich G.V., Podlesniy A.V. The near real-time diagnostics of ionosphere parameters at the middle point of the radio path on the base of oblique sounding data.*Proc. of SPIE*. 2015, vol. 9680, 96805E. DOI: 10.1117/12.2203589.

Song H., Hu Y., Jiang C., Zhou C., Zhao Z., Zou X. An automatic scaling method for obtaining the trace and parameters from oblique ionogram based on hybrid genetic algorithm. *Radio Sci.* 2016, vol. 51, no 12, pp. 1838–1854. DOI: 10.1002/2016RS005987.

Vertogradov G.G., Uryadov V.P., Vertogradova E.G. Calculation of optimal operating frequencies of a communication radio line according to oblique ionosphere sounding. *Radiophysics and Quantum Electronics.* 2008, vol. 51, iss. 1, pp. 9–19.

Uryadov V.P., Kurkin V.I., Vertogradov G.G., Vertogradov V.G., Ponyatov A.A., Ponomarchuk S.N. Features of propagation of HF signals on mid-latitude paths under conditions of geomagnetic disturbances. *Radiophysics and Quantum Electronics*. 2004, vol. 47, no.12, pp. 933–946.

URL: http://ckp-rf.ru/ckp/3056/ (accessed January 15, 2024).

Original Russian version: Ponomarchuk S.N., Grozov V.P., published in Solnechno-zemnaya fizika. 2024. Vol. 10. Iss. 2. P. 109–118. DOI: 10.12737/szf-102202410.

How to cite this article

Ponomarchuk S.N., Grozov V.P. Automatic interpretation of oblique sounding ionograms based on hybrid algorithms. *Solar-Terrestrial Physics*. 2024. Vol. 10. Iss. 2. P. 102–110. DOI: 10.12737/stp-102202410.